Time-Dependent Modelling of Single-Electron Interferometry with Edge-States

2015 J. Phys.: Conf. Ser. 647 012023

(http://iopscience.iop.org/1742-6596/647/1/012023)

Time-Dependent Modelling of Single-Electron Interferometry with Edge-States

A Beggi[1], **A Bertoni**[2], **P Bordone**[1,2]

[1] Dipartimento di Scienze Fisiche, Informatiche e Matematiche, Università degli Studi di Modena e Reggio Emilia, Via Campi 213/A, I-41125 Modena, Italy
[2] S3, Istituto Nanoscienze-CNR, Via Campi 213/A, I-41125 Modena, Italy

E-mail: andrea.beggi@unimore.it

Abstract. We simulate the time-resolved dynamics of localized electrons in a 2DEG system, where an external magnetic field creates quantum Hall edge states, and properly polarized split gates define a Mach-Zehnder electron interferometer. The carriers travelling inside the Hall channels consist of localized wave packets of edge states: they are propagated numerically by means of a Fourier split-step approach. We find that the energy-dependent scattering process at the quantum point contacts, together with the finite energy distribution of the carriers, have a remarkable effect on the transmission coefficient T of the device. We provide an analytical model to justify the characteristics of T which is in good agreement with the numerical simulations.

1. Introduction

Many recent theoretical and experimental works [1, 2, 3, 4] in the field of electron interferometry rely on edge states (ESs) in the integer quantum Hall regime as perfect 1D channels for coherent carrier transport. Indeed, these channels are highly immune to scattering and decoherence, thus being a good candidate as semiconductor quantum bits. The long-term aim of our work is devising solid-state flying qubits consisting of carriers travelling in ESs, and quantum logic gates based on quantum point contacts (QPCs) and a suitable pattern of surface split-gate designing a network of Hall edge channels. Here, we simulate the coherent propagation in time of electrons in a modulation-doped 2D device, where an applied orthogonal magnetic field creates ESs, and properly polarized split gates define a Mach-Zehnder electron interferometer (MZI). The electrons travelling inside the device are described by localized wave packets (WPs) of ESs. This, as already proposed in the literature [5, 6], is in contrast with the time-independent approach that deals with a single-energy delocalized edge state, thus losing the possibility to describe the explicit dynamics and the single-carrier evolution of the system.
In particular, our study is focused on the energy dependence of the transmission of the QPCs: since our carriers have a finite distribution of energies, this dependence has a remarkable impact on the total transmission coefficient T of the mesoscopic MZI. The results of numerical simulations are supported by a simplified exactly solvable analytical model.

2. Numerical Simulations

The Hall ESs of a 2DEG are chiral delocalized states that follow the boundary between a low-potential and a high-potential region of the device (respectively, allowed and forbidden for electrons). Their wave function has the form $\Psi_n(x, y, k) = \varphi_{n,k}(x)e^{iky}$, with travelling direction y and where the localized wave function $\varphi_{n,k}(x)$ depends on the details of the confining potential profile in the x direction. As a first step, we compute numerically $\varphi_{n,k}(x)$ by solving the effective Hall 1D Hamiltonian (with n and k being the index of the Landau level and the k-vector of

the ES, respectively) in the initialization region, where the split-gates potential is independent on y. Since the state $\Psi_n(x, y, k)$ can not represent localized particles, in order to describe a single-carrier travelling inside the MZI of Fig. 1, we consider a superposition of different ESs (belonging to the first Landau level, i.e. $n = 1$) with gaussian weights, that is:

$$\Psi_0(x, y) = \int dk\, F_\sigma(k)\varphi_{1,k}(x)e^{iky}, \tag{1}$$

where $F_\sigma(k) = \sqrt{\sigma}\,(2\pi)^{-3/4}\, e^{-\sigma^2(k-k_0)^2} e^{-iky_0}$. This wave function is indeed the ES equivalent of a minimum uncertainty WP of plane waves. Therefore, it represents a carrier which is initially localized around $x_0 = -\hbar k_0/eB$ and y_0. It is composed by ES with different momenta around $k = k_0$, and its group velocity is $v_g = \hbar k_0/m^*_B$.

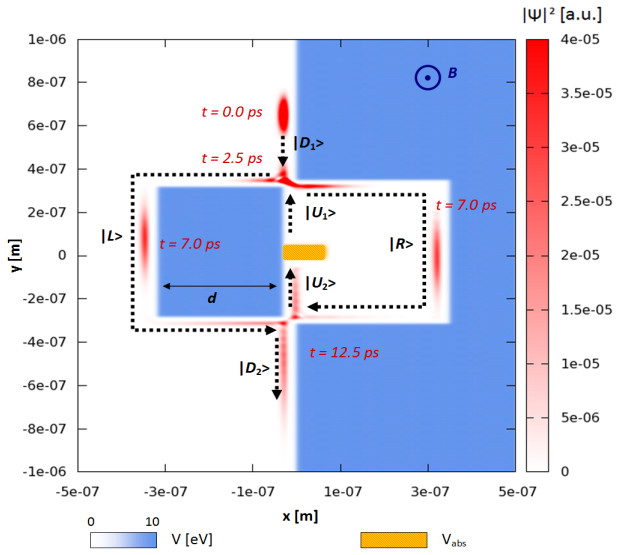

Figure 1. The MZI (in blue) used in our simulations, with snapshots of the electronic wavepacket (in red) at different times t. Dashed lines represent delocalized scattering states. The dimension d is changed in order to control Δl.

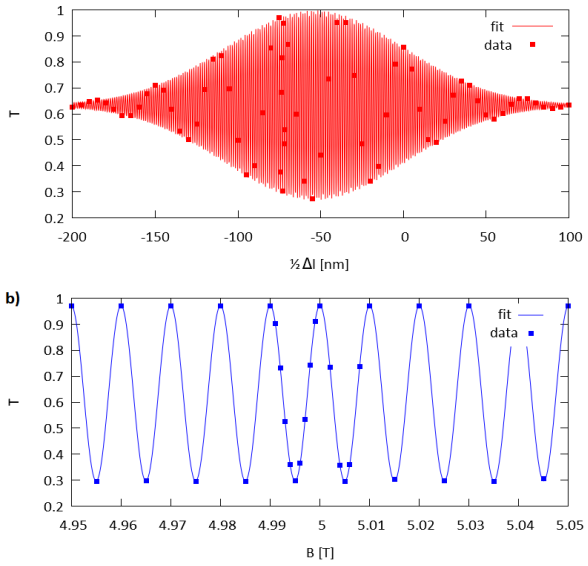

Figure 2. Transmission coefficient T obtained by fitting the results of time-dependent simulations: **a)** at a constant magnetic field B = 5 T and variable length mismatch ; **b)** at a constant length mismatch and variable magnetic field (Δl = -75 nm).

Our MZI device operates at filling factor $\nu = 1$. In detail, we model the edges of the split-gate pattern through smooth potential barriers (i.e. Fermi functions), and we tune the gap of both QPCs (the constrictions of the potential V in Fig. 1) in order to have a perfectly half-reflecting behaviour in terms of transmitted and reflected electron density (see Ref.[7] for other details on the device). In our simulations, the electron WP is split by the first QCP into two parts, that travel along the two arms of the device; then they are recollected and interfere at the second QPC, giving a transmitted and a reflected component. The latter is absorbed by a metallic lead, which is modeled with an imaginary potential V_{abs} (yellow rectangle in the center of Fig. 1). Therefore, the norm of the final WF is the transmission coefficient T of the device.
To solve the time-dependent Schrödinger equation including the external magnetic field B, we use a parallel Trotter-Suzuki scheme and the split-step Fourier method[8]. Simulations are performed for WPs of different initial extension, namely σ = 20 nm, 40 nm, and 60 nm (to obtain an optimal proportion between σ and the dimension of the device).
By changing the value of B or the area of the device (the latter is achieved by tailoring the length of one of the MZI arms), the transmission coefficient T shows Aharonov-Bohm oscillations, as

Initial WP	a) Fit of simulations			b) Analytical model			c) Numerical model		
σ (nm)	T_0	T_1	Σ (nm)	T_0	T_1	Σ (nm)	T_0	T_1	Σ (nm)
20.0	0.737	0.240	41.0	0.710	0.254	39.4	0.760	0.240	39.7
40.0	0.633	0.365	54.5	0.681	0.381	52.5	0.636	0.364	52.7
60.0	0.578	0.422	71.0	0.609	0.435	68.9	0.579	0.421	69.1

Table 1. Parameters for the transmission coefficient $T(\Delta l)$: **a)** from a fit of numerical simulations; **b)** from the analytical model; **c)** from numerical integration of Eq. (3).

reported in Fig. 2, in agreement with Ref[3]. However, when the lengths of the two paths become very different, we observe that the oscillations of the transmission are modulated by a gaussian envelope (see Fig. 2a), which is clearly a direct consequence of the finite-size of the electron WP. This has been already noted in literature[5]: once the length mismatch Δl between the two arms is substantially larger than σ, the two parts of the WF arrive at the second QPC at different times, and cannot interfere.

From a phenomenological point of view, the profile of $T(\Delta l)$ can be fitted with the following expression: $T(\Delta l) = T_0 + T_1 \exp(-\frac{1}{8}(\Delta l + c)^2/\Sigma^2)\cos(k_e \Delta l + \varphi_0)$. The fit parameters for our simulation are reported in columns a) of Table 1, for different dispersions of the initial WP. The visibility[1] $v_{MZI} = T_1/T_0$ is never ideal (i.e. unitary), but it increases as σ grows. Moreover, the amplitude of the gaussian damping of T, which is described by the standard deviation Σ, increases with σ. These effects can be understood by considering that the scattering process at the QPCs is k-dependent.

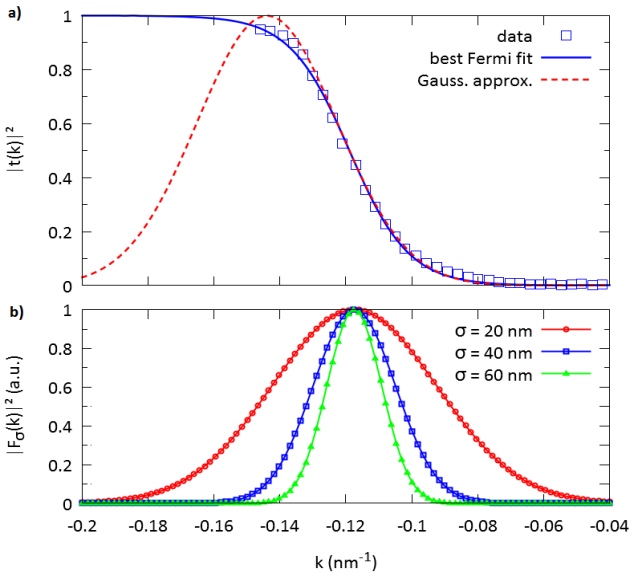

Figure 3. a) Transmission coefficient $|t(k)|^2$ for the first QPC: numerical calculations (points), Fermi fit (continuous line) and Gaussian approximation (dashed line). **b)** Gaussian weight distribution $|F_\sigma(k)|^2$ for the simulated WPs.

In order to evaluate these effects, we focus on the scattering process at the first QPC and analyze the reflected and the transmitted components of the WP by projecting them on the local set of ESs to get their spectral composition. Then, by comparing them with the initial WP, the numerical calculation of reflection and transmission probabilities at different k is straightforward: if the reflected WP contains the ES of momentum k with a probability $|F^r_\sigma(k)|^2$, then the reflection probability is $|r(k)|^2 = |F^r_\sigma(k)|^2/|F_\sigma(k)|^2$. A similar calculation can be made for $|t(k)|^2$.

The results of this calculation are shown in Fig. 3a, where the energy-dependence of the scattering amplitude t is evident. We found out that this behaviour is well described by a Fermi function $t(k) = (\exp(+\alpha(k-k_0))+1)^{-\frac{1}{2}}$ (and $r(k) = (\exp(-\alpha(k-k_0))+1)^{-\frac{1}{2}}$ for the reflection coefficient, not shown in the figure). We used the same fitting parameters for r and t in order to satisfy the constraint $|r(k)|^2 + |t(k)|^2 = 1$, and to get a perfect half-reflecting behaviour for $k = k_0$, namely the central wave vector of our WP.

3. Analytical Model

In order to develop an analytical model for the transmission of our MZI, able to take into account the energy dependence of the 2D scattering process in the QPCs, we note that the Fermi function

fitting the simulation data of Fig. 3a can be approximated by a Gaussian in the region around the turning point k_0, $(\exp(\alpha(k-k_0))+1)^{-1} \simeq \exp\left(-(\alpha(k-k_0)+\gamma)^2/4\gamma\right)$, with $\gamma = 4\ln(2)$. This approximation is acceptable in the range of k-components of our WPs, at least for $\sigma = 40\,\mathrm{nm}$ and $\sigma = 60\,\mathrm{nm}$ (see Fig. 3b).

We describe the dynamics of the wavepacket inside the MZI with the scattering matrix formalism[1]. The scattering states are represented in Fig. 1. The initial state is described by $|\Psi_0\rangle = \int dk\, F_\sigma(k)\,|D_1(k)\rangle$, while the scattering matrices of the QPCs, which are identical, are given by:

$$S = \begin{pmatrix} r(k) & it(k) \\ it(k) & r(k) \end{pmatrix}. \tag{2}$$

While travelling along the arms of the device, the phase acquired by the wavefunction is described by the matrix $P = \mathsf{diag}\left(e^{i\Delta\varphi}, 1\right)$, where $\Delta\varphi(k) = e\Phi_m/\hbar - k\cdot\Delta l$. Here, Φ_m is the magnetic flux of B through the device. The wavefunction after the scattering process is given by $|\Psi_f\rangle = SPS\,|\Psi_0\rangle$, and the norm of the transmitted part $|\Psi_T\rangle = \left(\frac{1}{2\pi}\int dk\ |D_2(k)\rangle\langle D_2(k)|\right)|\Psi_f\rangle$ gives the transmission coefficient T:

$$T = \frac{1}{2\pi}\int dk\ |F_\sigma(k)|^2\,|r^2(k)e^{i\Delta\varphi(k)} - t^2(k)|^2. \tag{3}$$

Using the Gaussian approximation for the transmission and reflection amplitudes, we can integrate analytically the previous expression, to get:

$$T = T_0 - T_1 e^{-\frac{\Delta l^2}{8\Sigma^2}}\cos\left(\frac{e}{\hbar}\Phi_m - k_0\Delta l\right), \tag{4}$$

where T_0 and T_1 – which represent, respectively, the average value of T and the maximum amplitude of its oscillations – are given by $T_0 = 2\frac{\sigma}{\Sigma}\exp\left(-\frac{\gamma\sigma^2}{2\Sigma^2}\right)$ and $T_1 = \frac{1}{2}\frac{\sigma}{\Sigma}$, while the standard deviation Σ is given by $\Sigma = \sqrt{\sigma^2 + \alpha^2/4\gamma}$.

As a consequence, the visibility is given by $v_{MZI} = \frac{1}{4}\exp\left(\gamma\sigma^2/2\Sigma^2\right)$, and we recover the ideal behaviour in the limit for $\sigma \to \infty$. Equation (4) predicts the same trend found in numerical simulations for T. If we used the energy-independent approximation, that is $r(k) = t(k) = 1/\sqrt{2}$, we would have obtained an expression for T which is formally identical to Eq. (4), but with $T_0 = T_1 = 1/2$ and $\Sigma = \sigma$: a result which is not consistent with our numerical simulations. Indeed, the gaussian damping Σ is not proportional to σ, as we observed in the numerical simulations, since there is a correction due to the scattering properties of the QPCs. Therefore, it is sufficient to include the localized nature of the carrier to recover the simulation results. However, in order to quantify the exact extension of this damping, as well as to justify the observed reduction in visibility with respect to the ideal case, we have to take into account the energy-dependent scattering at the QPCs. With this correction, the results of the numerical simulations are well reproduced by the analytical model (see Table I, columns a) and b)). Finally, we mention that a better agreement can be obtained with a direct numerical integration of Eq. (3), at the expense of an exact analytical solution. This result is reported in column c) of Table 1 and detailed in Ref.[7].

References

[1] Weisz E, Choi H K, Sivan I, Heiblum M, Gefen Y, Mahalu D and Umansky V 2014 **344** 1363–1366
[2] Bocquillon E, Freulon V, Berroir J M, Degiovanni P, Plaçais B, Cavanna A, Jin Y and Fève G 2013 **339** 1054–1057
[3] Neder I, Ofek N, Chung Y, Heiblum M, Mahalu D and Umansky V 2007 *Nature* **448** 333–337
[4] Fève G, Mahe A, Berroir J M, Kontos T, Placais B, Glattli D, Cavanna A, Etienne B and Jin Y 2007 *Science* **316** 1169–1172
[5] Haack G, Moskalets M, Splettstoesser J and Büttiker M 2011 *Phys. Rev. B* **84**(8) 081303
[6] Gaury B, Weston J and Waintal X 2014 *Phys. Rev. B* **90**(16) 161305
[7] Beggi A, Bordone P, Buscemi F and Bertoni A 2015 *arXiv preprint arXiv:1504.03837*
[8] Kramer T, Heller E J and Parrott R E *Journal of Physics: Conference Series*